Step changes in CO_2, Antarctic temperature and global climate during Termination II

A. Landais[1], G. Dreyfus[1,2,B], E. Capron[1,3], J. Jouzel[1], V. Masson-Delmotte[1], D.M. Roche[1,4], F. Prié[1], N. Caillon[1], J. Chappellaz[5], M. Leuenberger[6], A. Lourantou[5,1], F . Parrenin[5], D. Raynaud[5], G. Teste[5]

[1] Institut Pierre-Simon Laplace/Laboratoire des Sciences du Climat et de l'Environnement, UMR 8212, CEA-CNRS-UVSQ, 91191, Gif-sur-Yvette, France.

[2] Department of Geosciences, Princeton University, Princeton, NJ 08540, USA

[B] Now U.S. Department of Energy, Office of International Affairs, 1000 Independence Avenue SW, Washington, DC 20585, USA

[3] British Antarctic Survey, High Cross, Madingley Road, Cambridge, CB3 0ET, United Kingdom

[4] Earth & Climate Cluster, Faculty of Earth and Life Sciences, Vrije Universiteit Amsterdam, Amsterdam, The Netherlands

[5] UJF – Grenoble 1 / CNRS, Laboratoire de Glaciologie et Géophysique de l'Environnement (LGGE) UMR 5183, Grenoble, F-38041, France.

[6] Climate and Environmental Physics, Physics Institute, and Oeschger Centre for Climate Change Research, University of Bern, Sidlerstrasse 5, CH-3012 Bern, Switzerland.

Abstract

Deciphering the mechanisms linking glacial-interglacial climate dynamics and atmospheric CO_2 concentration has largely focused on the last termination (Termination I), where high resolution records and accurate chronologies are available. The observed sequences of events suggest simultaneous Northern Hemisphere cooling, Asian weak monsoon interval, CO_2 rise and Antarctic warming. Here, we present new high resolution records of atmospheric composition and climate from the air trapped in the EPICA Dome C ice core spanning Termination II. Using a proxy for climate in the gas record allows direct comparison with changes in atmospheric composition on a common age scale. While CO_2 and Antarctic temperature started increasing in phase at around 136 thousands of years before present (ka BP), an unequivocal lag of CO_2 vs Antarctic temperature is evidenced at the mid-slope of Termination II. This decoupling between Antarctic temperature and CO_2 is related to a two-step structure of Termination II with a decoupling between CO_2 and Antarctic temperature over the second phase (130.5 to 129 ka BP) of Termination II. This second phase coincides with an intensification of the low latitude hydrological cycle and we suggest that a low latitude CO_2 sink counteracted the CO_2 outgassing from the austral ocean over this period.

The penultimate deglaciation (from about 136 to 129 ka BP) occurred under a different climatic and orbital context than the last deglaciation, characterized by larger glacial Euroasian ice sheets[1], a larger eccentricity and a different phasing between precession and obliquity[2]. The European Project for Ice Coring in Antarctica Dome C (EDC) ice core is ideally suited to identify the mechanisms at play during this time period thanks to the detailed climate and atmospheric composition information archived within about 100 m of ice. Ice cores record variations in local temperature through water stable isotopes in the ice phase, and variations in global atmospheric composition (e.g. CO_2 and CH_4 concentrations) in the gas phase. Estimates of the age difference between the ice and the entrapped air are associated with uncertainties reaching several centuries[3]. In order to circumvent this difficulty, a profile of $\delta^{15}N$ in N_2 has been measured with an average resolution of 200 years for the period covering Termination II and the last interglacial period (~136-115 ka on the EDC3 timescale[4], Supplementary Online Material, SOM, Figure 1).

Changes in $\delta^{15}N$ reflect past variations of firnification processes, largely driven by local temperature and accumulation, itself strongly linked to temperature in central Antarctica (see, SOM). Our data reveal a very close correlation (R^2 =0.85) between the $\delta^{15}N$ gas record and the ice

δD, a proxy of local precipitation-weighted condensation temperature. This correlation is improved (R^2=0.89) when correcting δD for changes in oceanic moisture sources[5] (Figure 1). Following Caillon et al.[6] and Dreyfus et al.[7], this change in $\delta^{15}N$ is assumed to be driven by a change in surface temperature and/or accumulation rate, giving access to changes in polar climate recorded in the same gas phase as changes in global atmospheric composition. Our assumption of concomitant changes in $\delta^{15}N$, Antarctic surface temperature and/or accumulation rate is consistent with the use of $\delta^{15}N$ as an indicator of the gas lock-in depth[8] which allows, after correction for ice thinning, a direct estimate of the ice age – gas age difference during Termination I (see SOM). The latter approach cannot however be applied for Termination II due to increasing uncertainty on ice thinning with depth. Using $\delta^{15}N$ as a climate proxy allows a precise quantification of leads and lags between changes in Antarctic climate and in atmospheric composition during Termination II. Existing CO_2 and CH_4 data[9, 10] from the same EDC ice core were therefore complemented by new measurements to improve the resolution of the CO_2 record, and to characterize high resolution variations of $\delta^{18}O_{atm}$ of O_2, a complex tracer integrating changes in global sea level, hydrological cycle and biosphere productivity[11] (Figure 2).

The comparison of the evolutions of the CO_2 concentration and Antarctic temperature reveals two distinct phases within Termination II. Phase II-a is characterized by a parallel increase in CO_2 and Antarctic temperature. It is followed by phase II-b where atmospheric CO_2 concentration stabilizes around 260 ppm, preceding an abrupt increase to 285 ppm marking the end of Phase II-b and the onset of the last interglacial. During phase II-b, the rate of Antarctic temperature increase is reduced compared to Phase II-a. Our high resolution records thus evidence a decoupling between the dynamics of CO_2 and Antarctic temperature over the two phases of Termination II. Within the uncertainty linked with the data resolution and variability, the onsets of deglacial $\delta^{15}N$ and CO_2 changes occur simultaneously. At mid-slope, there is an unequivocal lead of $\delta^{15}N$ over CO_2 of 900 ± 325 years. This lead is slightly reduced to 675 ± 350 years when considering the radiative forcing caused by changes in CO_2 (see SOM). This different behaviour of CO_2 and Antarctic temperature contrasts with CO_2 evolving in parallel with Antarctic temperature over Termination I[12,13]. While earlier studies relying on firn models had reported a significant lead of Antarctic temperature on CO_2 during Termination I (e.g. 800±600 years[14]), the latest study using $\delta^{15}N$ data to constrain the gas ice – ice age difference[13] has depicted synchronous rise in CO_2 and Antarctic temperature at the beginning of the Termination and a lead of Antarctic temperature by 260 ± 130 years only at the beginning of the Bølling-Allerød (B/A). Over Termination III, an average lead of 800 years of Antarctic temperature on CO_2 was identified using a methodology similar to ours[6] but the low resolution of the records did not allow to assess the stability of this lead

through time. From the differences between the high resolution records of Termination I and Termination II, we conclude that Antarctic temperature and CO_2 are less closely related during Termination II than during Termination I.

Different mechanisms have been proposed to explain the simultaneous increase of CO_2 and Antarctic temperature over Terminations, consistent with the sequence of events over Termination I[15]. The first one describes Terminations as a super Dansgaard-Oeschger (D/O) event[16] with AMOC change leading to a bipolar see-saw[17]. In this view, North Atlantic cooling is associated with Southern Ocean (and Antarctic) warming and associated outgassing of CO_2. The second one is based on atmospheric teleconnections with increased winter northern hemisphere sea-ice and concomitant southward shifts of ITCZ and southern westerly winds leading to both an outgassing of CO_2 in the Southern Ocean[18] and Antarctic warming. A third mechanism invokes brine formation on the Antarctic margins[19]. The maximum expansion of the Antarctic ice sheet could stop brine formation, leading to CO_2 outgassing leading to simultaneous Antarctic warming through the added greenhouse effect. All these mechanisms can explain parallel rises in CO_2 and Antarctic temperature observed during Termination I and Phase II-a of Termination II, but cannot account for a rise of Antarctic temperature without an associated increase in atmospheric CO_2 concentration as identified during Phase II-b. The transition between Phase II-a and Phase II-b is also identified by an inflection toward a significant rise in the $\delta^{13}C$ record of CO_2[9,20], likely reflecting (1) a change in AMOC strength, a northward shift of westerlies in the southern ocean and then reduced upwelling and CO_2 outgassing or (2) an increase in terrestrial or marine biological productivity[9,20,21,22].

To shed light on possible mechanisms at play during Phase II-b, we now take advantage of our $\delta^{18}O_{atm}$ record. $\delta^{18}O_{atm}$ depends on the isotopic composition of water used by marine and terrestrial plants for their respiration. It is therefore sensitive to changes in continental ice volume which control sea-water $\delta^{18}O_{sw}$ and indirectly all meteoric waters[23,24]. At precessional and millennial scales, strong similarities have recently been identified between $\delta^{18}O_{atm}$ and Chinese speleothem calcite $\delta^{18}O$, reflecting changes in the East Asian monsoon[24,25,26]. At these time scales, the low latitude hydrological cycle is therefore believed to control changes in $\delta^{18}O_{atm}$ through its impact on meteoric water isotopic composition and global oxygen production.

We first summarize the structure of $\delta^{18}O_{atm}$ changes along Termination I (Figure 3). During Heinrich Stadial 1 (HS 1)[27], $\delta^{18}O_{atm}$ shows a slight increase, very likely reflecting the fingerprint of the Weak Monsoon Interval[28]. It decreases at the onset of the B/A, assumed to coincide with the resumption of AMOC at the end of HS 1 and the end of WMI[15]. The first phase of Termination II (II-a) is associated with an increase of $\delta^{18}O_{atm}$. At the beginning of Phase II-b, $\delta^{18}O_{atm}$ stopped to increase thus marking a clear inflection point and is followed by a slow $\delta^{18}O_{atm}$ decrease over phase

II-b. This slow decrease, close to a plateau between 130 and 129 ka, coincides with the plateau of CO_2 concentration, when CH_4 concentrations remain intermediate but Antarctic temperature is rising. By analogy with Termination I (Phases I-a and I-b), this pattern of CH_4 and Antarctic temperature could be explained by a weak AMOC and reduced NH monsoons. However, the weak monsoon periods of Termination I (Phases I-a and I-b) are characterized by an increase in $\delta^{18}O_{atm}$, in contrast with the decreasing $\delta^{18}O_{atm}$ during Phase II-b.

Within age scale uncertainties, Phase II-b may correspond to the ~1.5 ka pause identified during the second half of Termination II[28, 29,30] in some deep sea sediment and sea-level records. In well dated and high resolution Chinese speleothem calcite $\delta^{18}O$ data[28,31] (Figure 2), Termination II is depicted by a first long weak monsoon phase (WMI-II, corresponding to HS 11) perhaps punctuated by a brief multi-centennial wet phase at 134 ka BP[28]. The abrupt end of Termination II is identified in a sharp decrease of calcite $\delta^{18}O$ at 129 ka BP[28]. Using the high resolution record from Sanbao cave[28], a first 1‰ step drop in calcite $\delta^{18}O$ precedes by about 1.5 ka the main sharp decrease of 3‰ at 129 ka BP (SB25, Figure 2). Consistent with the 2 ka uncertainty between the chronology of ice cores and speleothems over Termination II[32], we propose that the first Sanbao calcite $\delta^{18}O$ drop at 130.5 ka corresponds to the inflection point in $\delta^{18}O_{atm}$ and hence to the transition between Phases II-a and II-b.

Altogether, these paleoclimate records evidence a climate event which affected the global carbon and oxygen cycles as well as the global atmospheric composition over 1.5 to 2 ka before the end of Termination II. During Termination I, the relatively small lag between Antarctic temperature and CO_2 has been attributed to the response time of the ventilation of the Southern Ocean[13,19,21,22,33]. The same mechanism may be at play during Phase II-a, with a weak AMOC corresponding to a "Heinrich Stadial"[34] associated with Antarctic warming and CO_2 degassing from the Southern Ocean. Our new data however point to a different process during Phase II-b of Termination II, which has no analogue during Termination I.

We now investigate the processes which may explain the slowdown of the atmospheric CO_2 concentration when Antarctic temperature is rising, during Phase II-b. At the beginning of Phase II-b, the global $\delta^{18}O_{atm}$ and the calcite $\delta^{18}O$ record from Sanbao cave consistently point to an intensification of the Northern Hemisphere low latitude hydrological cycle. This water cycle intensification is possibly associated with a slightly strengthened AMOC and change in productivity (as suggested by $\delta^{13}C$ of CO_2 [20,21]) possibly corresponding to a transition from an "Heinrich stadial" to a "D/O stadial[34]" and/or a reduced Northern Hemisphere sea-ice extent. We propose that the change in low latitude climate enhanced the low latitude carbon sinks due to changes in the biosphere productivity and the ocean-atmosphere CO_2 exchange[35], which compensated the CO_2

degassing from the warming Southern Ocean, explaining the observed plateau of CO_2 concentration. The significant rise in $\delta^{13}C$ of CO_2 observed at that time[20] is in line with this interpretation, either through a low latitude carbon uptake process or resulting from a slight decrease in CO_2 deep water outgassing in the southern ocean following a northward shift of westerly winds[22].

The end of phase II-b and hence of Termination II is then characterized by a strong enhancement of the low latitude hydrological cycle, tracked by a steeper decreasing rate of $\delta^{18}O_{atm}$ and the large decrease of Sanbao Cave[28] calcite $\delta^{18}O$ probably coincident with a large AMOC strengthening. In our Antarctic records, it is clearly identified through an abrupt rise in CH_4, peak Antarctic temperature and CO_2 concentration. This final abrupt increase in CO_2 concentration is also concomitant with an abrupt shift in deuterium excess, a proxy of Antarctic moisture source shifts[36]. This suggests that the end of phase II-b is associated with an abrupt shift in southern westerlies favoring a final CO_2 outgassing from the southern ocean that is no longer counteracted by low latitude sinks.

Why are the sequences of events different during HS1-Termination I and HS11 – Termination II? These two terminations occur under different orbital contexts and the duration of HS 11 is estimated to have been twice longer than HS 1[27] (6 ka vs 3 ka). The higher eccentricity during Termination II strengthens the magnitude and rate of changes in Northern Hemisphere summer insolation, compared to Termination I[2]. Climate models relate freshwater fluxes and AMOC intensity. A stronger rate of retreat of the Laurentide ice sheet may therefore have maintained a reduced AMOC for a longer time during Termination II compared to Termination I, where an early AMOC recovery corresponding to the B/A is interrupted by HS0 leading to the Northern Hemisphere Younger Dryas cooling. Do these differences in AMOC histories have different impacts on the carbon cycle through different rates of southern ocean destratification and CO_2 outgassing? Does the orbital context of Termination II explain a larger response of the low latitude water cycle at the end of Termination II? The new questions unveiled thanks to the detailed global sequence of events during Termination II should be tested using Earth system models, expanding the possibility to test climate and carbon cycle mechanisms during two different transitions.

Additionnal informations:

Supplementary information is available in the online version of the paper. Correspondence and requests for materials should be addressed to A. La.

Authors contributions:

A.La., J.J. and V.M-D. formulated the project. A.La., G.D., E.C., F.Pr. and G.T. performed the measurements. A.La, G. D., E. C., J. J., V. M.-D., D.M.R., N. C., J. C., M. L., A. Lo, F . Pa. and D. R. performed the analysis and contributed to the writing and polishing of the manuscript.

Acknowledgments:

This work is a contribution to the European Project for Ice Coring in Antarctica (EPICA), a joint ESF (European Science Foundation)/EC scientific program, funded by the European Commission and by national contributions from Belgium, Denmark, France, Germany, Italy, the Netherlands, Norway, Sweden, Switzerland and the United Kingdom. The main logistic support was provided by IPEV and PNRA (at Dome C). The research leading to these results has received funding from the European Union's Seventh Framework program (FP7/2007-2013) under grant agreement n^{o} 243908, "Past4Future: Climate change - Learning from the past climate". This manuscript benefited from very constructive reviews of three referees as well as fruitful discussions with C. Waelbroeck, E. Michel, D. Paillard M.F. Sanchez-Goni, L. Bazin, M. Guillevic, H. Fischer and J. Schmitt.

References:

1 Lambeck, K. et al. Constraints on the Late Saalian to Early Middle Weichselian ice sheet of Eurasia from field data and rebound modelling. *Boreas* **35,** 539-575 (2006)

2 Berger, B. Long term variations of daily insolation and Quaternary climatic changes. *Journal of Atmospheric Sciences* **35(12),** 2362-2367 (1978)

3 Fischer, H., Wahlen, M., Smith, J., Mastroianni, D. & Deck, B., Ice Core Records of Atmospheric CO_2 Around the Last Three Glacial Terminations. *Science*. **283,** 1712-1714 (1999)

4 Parrenin, F. et al. The EDC3 agescale for the EPICA Dome C ice core. *Clim. Past* **3,** 485-497 (2007)

5 Stenni, B. et al. The deuterium excess records of EPICA Dome C and Dronning Maud Land ice cores (East Antarctica). *Quaternary Science Reviews* **29,** 146-159 (2010)

6 Caillon, N. et al. Timing of atmospheric CO2 and Antarctic temperature changes across Termination III. *Science* **299,** 1728-1731 (2003)

7 Dreyfus G.B. et al. Firn processes and $\delta^{15}N$: potential for a gas-phase climate proxy. *Quaternary Science Reviews* **29,** 222-234 (2010)

8 Parrenin, F. et al. On the gas-ice depth difference (Δdepth) at EPICA Dome C. *Clim. Past* **8,** 1239-1255 (2012).

9 Lourantou, A., Chappellaz, J., Barnola, J.-M., Masson-Delmotte, V. & Raynaud, D. Changes in atmospheric CO_2 and its carbon isotopic ratio during the penultimate deglaciation. *Quaternary Science Reviews* **29,** 1983-1992 (2010)

10 Loulergue, L. et al. Orbital and millennial-scale features of atmospheric CH4 over the past 800,000 years. *Nature* **453,** 383-386 (2008)

11 Bender, M., T. Sowers & Labeyrie L. The Dole Effect and its variations during the last 130,000 years as measured in the Vostok Ice Core, *Global Biogeochem. Cycles* **8,** 363–376 (1994)

12 Pedro, J. B., Rasmussen, S. O. & van Ommen, T. D. Tightened constraints on the time-lag between Antarctic temperature and CO_2 during the last deglaciation. *Clim. Past* **8,** 1213-1221 (2012)

13 Parrenin, F. et al. Zero phasing between CO_2 and Antarctic temperature during the last deglacial warming, *Science* **339,** 1060-1063 (2013)

14 Monnin, E. et al.,Atmospheric CO_2 concentrations over the last glacial termination. *Science* **291,** 112-114 (2001)

15 Denton, G.H. et al. The last glacial termination. *Science* **328,** 1652-1656 (2010).

16 Wolff, E.W., Fischer, H. & Rothlisberger, R. Glacial terminations as southern warmings without northern control. *Nature Geoscience* **2,** 206-209 (2009)

17 Broecker, W. S., Paleocean circulation during the Last Deglaciation: A bipolar seesaw?, *Paleoceanography*, **13,** 119–121 (1998)

18 Skinner, L. C., Fallon, S., Waelbroeck, C., Michel, E. & Barker, S. Ventilation of the deep southern ocean and deglacial CO_2 rise, *Science* **328**, 1147-1151 (2010)

19 Bouttes, N., Paillard D. & Roche, D.M. Impact of brine-induced stratification on the glacial carbon cycle, *Clim. Past* **6,** 575-589 (2010)

20 Schneider, R., Schmitt, J., Köhler, P., Joos, F. & Fischer, H. A high resolution record of atmospheric carbon dioxide and its stable carbon isotopic composition from the penultimate glacial maximum to the glacial inception, *Clim. Past Discuss.* **9,** 2015-2057 (2013)

21 Lourantou, A. et al. Constraint of the CO2 rise by new atmospheric carbon isotopic measurements during the last deglaciation. *Global Biogeochem. Cycles* **24,** GB2015 (2010)

22 Schmitt, J. et al. Carbon isotope constraints on the deglacial CO_2 rise from ice cores. *Science* **336,** 711-714 (2012)

23 Jouzel, J., Hoffmann, G., Parrenin, F., & Waelbroeck, C. Atmospheric oxygen 18 and sea-level changes. *Quat. Sci. Rev.* **21,** 307–314 (2002)

24 Severinghaus, J.P., Beaudette, R.A., Headly, M., Taylor, K. & Brook, E. J. Oxygen-18 of O2 Records the Impact of Abrupt Climate Change on the Terrestrial Biosphere. *Science* **324,** 1431-1434 (2009)

25 Wang Y. al. Millennial- and orbital-scale changes in the East Asian monsoon over the past 224,000 years. *Nature* **451,** 1090-1093 (2008)

26 Landais, A. et al. What drives the orbital and millennial variations of d18Oatm? *Quaternary Science Reviews* **292,** 235-246 (2010)

27 Barker, S. et al. Interhemispheric Atlantic seesaw response during the last deglaciation, *Nature* **457,** 1097-1102 (2009)

28 Cheng, H. et al. Ice Age Terminations. *Science* **326**, 248-251 (2009)

29 Gallup, C. D. , Cheng, H., Taylor, F.W. & Edwards, R.L. Direct Determination of the Timing of Sea Level Change During Termination II. *Science* **295,** 310-313 (2002)

30 Gouzy A., Malaize B., Pujol C. & Charlier K. Climatic -pause- during Termination II identified in shallow and intermediate waters off the Iberian margin, *Quaternary Science Reviews* **23,** 1523-1528 (2004)

31 Cheng, H., Edwards, R.L., Wang, Y., Kong, X. et al., A penultimate glacial monsoon record from Hulu Cave and two-phase glacial terminations: *Geology* **34,** 217–220 (2006)

32 Bazin, L. et al., An optimized multi- proxy, multi-site Antarctic ice and gas orbital chronology (AICC2012): 120–800 ka, *Clim. Past* **9,** 1715-1731 (2013)

33 Koehler, P.; Fischer, H. & Schmitt, J. Atmospheric delta (CO2) - C-13 and its relation to pCO(2)

and deep ocean delta C-13 during the late Pleistocene, Paleoceanography **25,** PA2216 (2010)

34 Alley, R., Anandakrishnan, S., and Jung, P.: Stochastic resonance in the North Atlantic. *Paleoceanography* **450,** 190–198 (2001)

35 Douville, E. et al., Abrupt sea surface pH change at the end of the Younger Dryas in the central sub-equatorial Pacific inferred from boron isotope abundance in corals (Porites), *Biogeosciences* **7,** 2445–2459 (2010).

36 Masson-Delmotte, V. et al. An abrupt change of Antarctic moisture origin at the end of Termination II. *PNAS* **107,** 12091-12094 (2010)

37 Jouzel, J. et al. Orbital and Millennial Antarctic Climate Variability over the Past 800,000 Years. *Science* **317,** 793-797 (2007)

Figure 1: Comparison of EDC $\delta^{15}N$ and T_{site} records on the EDC3 timescale.

T_{site} has been calculated from the combination of ice $\delta^{18}O$ and δD[8]. The vertical scales have been adjusted around the present-day levels of $\delta^{15}N$ and T_{site}. The horizontal dashed line indicates present-day levels of EDC $\delta^{15}N$ and T_{site}.

Figure 2: Sequence of events over Termination II

From top to bottom are displayed $\delta^{18}O_{calcite}$ from the Sanbao cave[25, 28] and EDC data records (CH_4[10],CO_2 [9] with new data in purple, $\delta^{15}N$[7] with new data in points, δD[4], $\delta^{18}O_{atm}$ measured at Princeton with open squares and at LSCE with points). The horizontal dashed grey line highlights the change of timescale between speleothem and ice core records. The grey arrow indicates the "interstadial" event identified in Sanbao cave record[27] during Termination 2. The ramps fitting CO_2 and $\delta^{15}N$ records (SOM) are indicated in light red and light blue respectively. Standard deviations are indicated as error bars on y-axis.

Figure 3 : Sequence of events over Termination I

From top to bottom are displayed EDC data records (CH_4[10], CO_2[9], δD[37], $\delta^{18}O_{atm}$). The location of HS 1 (Heinrich Stadial 1) is indicated[27] as well as phases I-a, I-b, I-c, I-d corresponding to phases 1, 2, 3, 4 of Monnin et al.[14].

Supplementary material to "Step changes in CO_2, Antarctic temperature and global climate during Termination II" by A. Landais et al.

1- Phase relationship between the CO_2 concentration and Antarctic temperature change during Termination II

Because past variations in atmospheric CO_2 concentrations are measured in the gas phase while the classical temperature proxy, δD, is measured in the ice phase of ice cores, evaluating their phase relationships requires quantification of the depth difference between a synchronous event recorded in the ice and gas phases (Δdepth) or the age difference between gas and ice at the same depth (Δage). This depth or age difference has commonly been estimated using firnification models[S1, S2, S3]. In low accumulation rate sites of central East Antarctica, independent Δdepth estimates have revealed that these models appear to systematically overestimate Δdepth under glacial conditions at these sites[S4, S5], challenging their use for estimating the CO_2-Antarctic temperature timing under glacial conditions.

The isotopic composition of nitrogen ($\delta^{15}N$ of N_2, hereafter $\delta^{15}N$) or argon ($\delta^{40}Ar$ of Ar) in air trapped in ice cores, can be used to assess past changes in Δdepth. Indeed, assuming that the firn structure remains roughly the same over glacial-interglacial changes (constant depth of convective zone, constant average firn density and constant vertical temperature gradient), $\delta^{15}N$ changes enable to estimate changes in lock-in depth (LID, where air no longer diffuses in the firn) during Termination I[S4]. Alternatively a record of $\delta^{40}Ar$ during Termination III was interpreted as an indicator of surface temperature and/or accumulation rate changes in the gas phase[S6]. The strong influence of accumulation rate on $\delta^{15}N$ evolution over deglaciation has been recently confirmed on a compilation of $\delta^{15}N$ measurements at different Antarctic sites[S5]. Over Termination III, Vostok temperature and/or accumulation rate changes were shown to lead changes in atmospheric CO_2 concentration by 800 ± 200 years on average.

Figure S1 displays the complete high-resolution $\delta^{15}N$ profile measured at the Laboratoire des Sciences du Climat et de l'Environnement (LSCE) over Termination II and the last interglacial period, consisting of 20 duplicated depth levels already published[S7] and 130 new depth levels measured in 2010 using a melt-refreeze method for air extraction and dual inlet mass spectrometry for measurements[S8] of $\delta^{15}N$ of N_2. The resulting uncertainty on $\delta^{15}N$

measurement over this series of measurements is of 5 ppm (1 σ). The average depth resolution is 2.75 m corresponding to an age resolution of 200 years over Termination II. We therefore reach a temporal resolution similar to that of available CO_2 measurements[S9] over Termination II and completed in this study by 12 additional measurements at the start of Termination II on the same ice core (Figure 1).

Using the EDC3 gas and ice timescales[S10,S11], δD and $\delta^{15}N$ are highly correlated (R^2 of 0.85**,** n= 150) with a lag of $\delta^{15}N$ with respect to δD by ~3 ka over the optimum of the last interglacial period. Polar precipitation δD is an integrated tracer of the water cycle, which is not only affected by changes in condensation temperature but also by changes in evaporation conditions (isotopic composition, surface temperature and humidity at evaporative sources). After accounting for source conditions using the second-order parameter deuterium excess, Stenni et al.[S12] have estimated changes in EDC site temperature (T_{site}). The comparison between T_{site} and $\delta^{15}N$ shows a slightly stronger correlation compared to the one obtained with δD (R^2=0.89, n=150). During the glacial inception, around 115 kyrs BP, $\delta^{15}N$ and T_{site} synchronously decrease (Figure 2). This comparison confirms the inference of Stenni et al.[S12] that δD is affected by warm source conditions at the glacial inception, which enhance isotopic depletion.

The good correlation between $\delta^{15}N$ and both δD and T_{site} on their EDC3 timescales supports a previous conclusion[S6,S7] that glacial-interglacial variations of $\delta^{15}N$ are driven by changes in surface temperature and/or accumulation rate. Accumulation rate changes in ice cores are assumed to be driven by variations of surface temperature through an exponential law[S13] and this general relationship between accumulation rate and temperature is in general agreement with layer counting measurements in Greenland ice cores[S14]. As a consequence, both accumulation rate and temperature variations are expected to be in phase with δD variations in ice cores. Recently, changes in dust content have been suggested to be an additional driver of snow metamorphism and firn depth[S15]. A recent compilation of coastal to central Antarctic $\delta^{15}N$ records spanning the last deglaciation did however not exhibit any obvious relationship between dust concentration and $\delta^{15}N$, while the correlations between $\delta^{15}N$ and δD variations were shown to be robust with an important influence of changes in accumulation rate on $\delta^{15}N$ variations[S5]. During Termination II, the onset of EDC dust concentration decrease coincides with the start of δD increase[S16, S17], hence at much shallower depth (30 m) than the start of the $\delta^{15}N$ increase which can therefore not be explained by the increase in dust concentration near the firn pore close-off. Moreover, the dust concentration

reaches an interglacial level quickly, about 2.5 ka before δD[S16, S17]. If dust concentration was the primary driver of $\delta^{15}N$, a decoupling between $\delta^{15}N$ and δD should be recorded during the intervals of large dust variations but this is not observed. Still, we cannot rule out a lag between changes in surface temperature / accumulation rate and $\delta^{15}N$ at firn close-off. However, we can safely consider that $\delta^{15}N$ did not change before and more rapidly than temperature / accumulation rate at the surface.

With these limitations in the interpretation of $\delta^{15}N$ in mind, we now compare $\delta^{15}N$ evolution over Termination II with the EDC record of CO_2 on the same depth scale (Table 1, Figure 3). Comparing the two evolutions is not easy because the rate of δD, $\delta^{15}N$ and CO_2 increases are not constant over Termination II. This is especially true for the end of Termination II where the rate of increase in $\delta^{15}N$ slows at ~1750 m (when interglacial $\delta^{15}N$ values are reached). $\delta^{15}N$ values then continue to increase slowly until the optimum of MIS 5.5 is reached at ~1716 m. In contrast CO_2 reaches a plateau between 1741 m and 1724 m before the overshoot occurring in phase with the $\delta^{15}N$ maximum at the MIS 5.5 optimum. Despite these slight differences in behaviors at the end of Termination II, we have chosen to use a determination based on the Rampfit software[S18] to compare objectively the onsets and mid-slopes of the main increases in levels of CO_2, $\delta^{15}N$, and δD (Table 1). We used depth windows of 1680 – 1840 m for the gas phase and 1620-1780 m for the ice phase (or the equivalent time windows).

While the onsets of $\delta^{15}N$ and CO_2 cannot be distinguished within the ~2 m uncertainty, we see a clear lead of $\delta^{15}N$ over CO_2 at the mid-slope (10.2 ± 3.6 m) of the main increasing phase of Termination II. This lead is not modified if we remove the CO_2 inflexion point at 1741.3 m and the associated error bar is only increased by 0.17 m. The rate of increase in $\delta^{15}N$ is thus greater than for CO_2 resulting in $\delta^{15}N$ achieving its mid-points ahead of CO_2. This result is robust regardless of differences in behavior of these two parameters during the last interglacial, as discussed above. Over the last part of the Termination II, quantifying the visible lead of $\delta^{15}N$ over CO_2 is not easy since both signals show a different dynamic with a slow and rather constant increase for $\delta^{15}N$ versus a plateau followed by an overshoot for CO_2.

Assuming that the firn structure did not change over time (no convective zone)[S19], $\delta^{15}N$ can be used as an indicator of LID. We therefore apply the method proposed by Bender et al.[S20] and Parrenin et al.[S4] to Termination II at EDC. The depth difference, Δdepth, between

concomitant change in gas and ice phases is calculated[S4] from (i) the thinning value at the depth of Termination II and (ii) the lock-in depth inferred from $\delta^{15}N$ and the barometric equation. The main limitation of this approach lies in the ~10 % uncertainty in the thinning function at 1700 m depth, which leads to a 3.5 m uncertainty on the Δdepth calculation. While this uncertainty prevents us from firm conclusions on the mid-slope lead or lag of CO_2 vs temperature, we note that the shape of the δD increase, when shifted by Δdepth, is very close to the $\delta^{15}N$ increase (difference of 2 m) which supports our use of $\delta^{15}N$ as a proxy for δD in the gas phase. The same exercise has been done over Termination III at Vostok comparing the results obtained by Caillon et al.[S6] and our Δdepth approach using in this case a convective zone of 13 m as for present-day Vostok conditions[S20]. Again the two approaches give similar results despite large uncertainties in the Δdepth approach (Figure S4).

Finally, our most robust finding is that the initial increase in $\delta^{15}N$ and CO_2 occur synchronously, within uncertainty, and that the mid-slope of $\delta^{15}N$ increase (which cannot precede changes in temperature and accumulation over Termination II as discussed above through its link with δD or T_{site} and timing of dust increase) occurs prior to the mid-slope of CO_2 increase. At mid-slopes, the increase in $\delta^{15}N$ leads by 900 ± 325 years those of CO_2. We know from modeling studies that Antarctic temperature is not a linear function of CO_2 concentration[S21]. This is due to the following logarithmic relationship[S22] between radiative forcing (RF) and the atmospheric concentration of CO_2.

$RF\ (W.m^{-2}) = 5.35\ \ln(CO_2/CO_{2,0})$ with $CO_{2,0} = 278$ ppm. (Equation 1)

We have thus repeated our ramp analysis using the radiative forcing of CO_2 (Table S1) deduced from Equation (1). In this case, $\delta^{15}N$ still leads CO_2 radiative change by 675 ± 350 years at mid-slope.

2- High resolution measurements of $\delta^{18}O_{atm}$ over Termination I and Termination II.

$\delta^{18}O$ of O_2 is measured on the same samples than $\delta^{15}N$ of N_2. For measurements performed at LSCE, the same melt-refreeze method is used[S8] and the same dual inlet mass spectrometer run measures $\delta^{15}N$ of N_2 and $\delta^{18}O$ of O_2 using a Thermo Delta V equipped with masses 28, 29, 30, 32, 33, 34 and 44. For measurements performed at Princeton, the headspace equilibration method inspired from Emerson et al.[S23] and improved by Dreyfus et al.[S7] has

been applied. Simultaneous measurements of $\delta^{15}N$[S7] and $\delta^{18}O$ were achieved using a Delta Plus XP mass spectrometer. For both sets of measurements, corrections for CO^+ influence on mass 28 and for influences of the $\delta O_2/N_2$ on $\delta^{15}N$ and $\delta^{18}O$ values are done[S8,S24].

A gas loss effect has been shown to influence measurements of both $\delta^{18}O$ of O_2 and $\delta O_2/N_2$ in air trapped in ice core with a constant slope[S25,S26,S27,S28] of 0.01‰/‰ between the changes in $\delta O_2/N_2$] so that the corrected $\delta^{18}O$ of O_2 is calculated as[S29]:

$$\delta^{18}O_{corr} = \delta^{18}O_{measured} + (\delta O_2/N_2 + 10) \times 0.01$$

To separate the firn and atmospheric fractionation processes, the influence of gravitational fractionation in the firn is removed from corrected $\delta^{18}O$ of O_2 using the $\delta^{15}N$ measurements so that:

$$\delta^{18}O_{atm} = \delta^{18}O_{corr} - 2\,\delta^{15}N$$

The final uncertainty attached to $\delta^{18}O_{atm}$ values at each level is of 0.025 ‰ (1 σ) for the series of data from Termination II and Termination I presented here.

3- Measurements of CO_2 concentration

The CO_2 data plotted on Figure 2 include 2 sets of measurements. The first set was obtained from the published data by Lourantou et al.[S9] while the second one has been obtained for this study. The same extraction method has been used in both cases, i.e. 40 – 50g of ice are placed under vacuum and crushed in a steel ball mill.

In the case of the Lourantou et al.[S9] set, CO_2 and its carbon isotopic ratio measurements are coupled. The extracted gas is expanded in a 10 cm^3 sample loop. From there, an ultra pure helium stream flushes the gas through a glass trap where CO_2 is frozen out at−196 °C. The trapped CO_2 is then transferred into a low flow rate helium stream, to be cryofocused on a small volume glass capillary tubing also at −196 °C. The subsequent warming of the capillary allows the gas transfer through a gas chromatograph to separate the CO_2 from residual impurities such as N_2O and its introduction in the isotope ratio mass spectrometer IRMS (Finnigan MAT 252). The CO_2 mixing ratio in the ice samples is deduced from a linear regression between standard gas injections (CO_2 = 260.26 ± 0.2 ppmv in dry air) at different

pressures and the corresponding CO_2 peak amplitude measured by the IRMS. Each sample or external standard introduction in the IRMS is bracketed with injections of a pure CO_2 standard reference gas (internal standard, ATMO MESSER, $\delta^{13}C$ of−6.5 ± 0.1‰ versus VPDB). Each result of ice core gas sample consists of the mean of three consecutive measurements of the same sample gas stored in the extraction container and expanded three times. For this analytical series on Termination II EDC samples, the pooled standard deviation associated with the average value of three replicate measurements of the same extracted gas amounts to 1.9 ppmv for CO_2.

In the case of the new set of measurements (this work), the extracted gas is expanded in a 1 cm^3 sample loop and flushes with an ultra pure helium stream through inox tubing line. A Gas Chromatograph (GC) Varian 3300 separates the CO_2, reduces it to CH_4 through a methanizer, and with a Flame Ionised Detector produces an electrical signal proportional to the concentration. The CO_2 mixing ratio is deduced using the same protocol as Lourantou et al. We use a linear regression between standard gas injections (CO_2 = 232.6 ± 0.2 ppmv) at different pressures and the corresponding CO_2 peak amplitude measured by the GC. Each ice core gas sample result is calculated as the mean of minimum 4 replicate measurements of the same sample gas stored in the extraction cell. The standard deviation associated with the average value of replicate measurements amounts to 1.3 ppmv.

We note the good agreement between the 2 sets of measurements, which have been obtained with 2 different analytical procedures.

References:

S1 Monnin et al. Atmospheric CO_2 concentrations over the last glacial termination. *Science* **291,** 112-114 (2001)

S2 Fischer, H., Wahlen, M., Smith, J., Mastroianni, D. & Deck, B., Ice Core Records of Atmospheric CO2 Around the Last Three Glacial Terminations. *Science* **283,** 1712-1714 (1999)

S3 Pedro, J. B., Rasmussen, S. O. & van Ommen, T. D. Tightened constraints on the time-lag between Antarctic temperature and CO_2 during the last deglaciation. *Clim. Past* **8,** 1213-1221 (2012)

S4 Parrenin, F. et al. On the gas-ice depth difference (Δdepth) at EPICA Dome C. *Clim. Past* **8,** 1239-1255 (2012).

S5 Capron, E. et al. Glacial-interglacial dynamics of Antarctic firn columns: comparison between simulations and ice core air-δ15N measurements. *Clim. Past Discuss* **8,** 6051-6091 (2012)

S6 Caillon, N. et al. Timing of atmospheric CO_2 and Antarctic temperature changes across Termination III. *Science* **299,** 1728-1731 (2003)

S7 Dreyfus G.B. et al. Firn processes and d15 N: potential for a gas-phase climate proxy. *Quaternary Science Reviews* **29,** 222-234 (2010)

S8 Landais A., Caillon, N., Severinghaus, J.P., Jouzel, J., & Masson-Delmotte,V. Analyses isotopiques à haute précision de l'air piégé dans les glaces polaires pour la quantification des variations rapides de température : méthode et limites. *Notes des Activités Instrumentales de l'IPSL* **39,** 1-15 (2003)

S9 Lourantou, A., Chappellaz, J., Barnola, J.-M., Masson-Delmotte, V. & Raynaud, D. Changes in atmospheric CO_2 and its carbon isotopic ratio during the penultimate deglaciation. *Quaternary Science Reviews.* **29,** 1983-1992 (2010)

S10 Parrenin, F. et al. The EDC3 agescale for the EPICA Dome C ice core. *Clim. Past* **3,** 485-497 (2007).

S11 Loulergue, L. et al. New constraints on the gas age-ice age difference along the EPICA ice cores, 0–50 kyr. *Clim. Past* **3,** 527-540 (2007)

S12 Stenni, B. et al. The deuterium excess records of EPICA Dome C and Dronning Maud Land ice cores (East Antarctica). *Quaternary Science Reviews* **29,** 146-159 (2010)

S13 Lorius, C., Merlivat, L. & Hagemann, R. Variation in mean deuterium content of precipitations in Antarctica. *Journal of Geophysical Research* **74,** 7027-7037 (1969)

S14 Rasmussen, S.O. et al. Synchronization of the NGRIP, GRIP, and GISP2 ice core across MIS 2 and palaeoclimatic implications. *Quaternary Science Reviews* **27,** 18-28 (2008)

S15 Hörhold, M. W. et al. On the impact of impurities on the densification of polar firn. *Earth and Planetary Science Letters* ***325*****,** 93-99 (2012)

S16 Lambert F. et al. Dust-climate couplings over the past 800,000 years from the EPICA Dome C ice core. *Nature* **452,** 616-619 (2008).

S17 Röthlisberger, R. et al. The Southern Hemisphere at glacial terminations: insights from the Dome C ice core. *Climate of the Past* **4,** 345-356 (2008)

S18 Mudelsee, M. Ramp function regression: a tool for quantifying climate transitions. *Comput. Geosci.* **26,** 293–307 (2000)

S19 Landais, A. et al. Firn-air d15N in modern polar sites and glacial-interglacial ice: a model-data mismatch during glacial periods in Antarctica? *Quaternary Science Reviews* **25,** 49-62 (2006)

S20 Bender, M. L. et al. Gas age-ice age differences and the chronology of the Vostok ice core, 0-100 ka, *Journal of Geophysical Research - Atmospheres* **111,** D21115 (2006)

S21 Ganopolski, A. & Roche, D. On the nature of lead-lag relationships during glacial-interglacial climate transitions, *Quaternary Science Reviews* **37/38,** 3361-3378 (2009)

S22 Joos, F. Radiative forcing and the ice core greenhouse gas record. *PAGES Newsletters* **13/3**, 11-13 (2005)

S23 Emerson, S., Quay, P., Stump, C., Wilbur, D. & Schudlich, R. Chemical tracers of productivity and respiration in the subtropical Pacific Ocean. *J. Geophys. Res.* **100,** 15873–15887 (1995).

S24 Severinghaus, J. P., Grachev A. & Battle, M., Thermal fractionation of air in polar firn by seasonal temperature gradients. *Geochemistry, Geophysics, Geosystems*. **2,** 2000GC000146 (2001)

S25 Landais A. et al. A tentative reconstruction of the last interglacial and glacial inception in Greenland based on new gas measurements in the Greenland Ice Core Project (GRIP) ice core. *J. Geophys. Res.* **108,** 4563 (2003)

S26 Dreyfus, G. B. et al. Anomalous flow below 2700m in the EPICA Dome C ice core detected using 18O of atmospheric oxygen measurements. *Clim. Past* **3,** 341–353 (2007)

S27 Suwa, M. & Bender, M.L. O_2/N_2 ratios of occluded air in the GISP2 ice core. *J. Geophys. Res.* **113,** D11119 (2008).

S28 Severinghaus, J.P., Beaudette, R.A., Headly, M., Taylor, K. & Brook, E. J. Oxygen-18 of O_2 Records the Impact of Abrupt Climate Change on the Terrestrial Biosphere. *Science* **324,** 1431-1434 (2009)

S29 Landais, A. et al. What drives the orbital and millennial variations of $\delta^{18}O_{atm}$? *Quaternary Science Reviews* **292,** 235-246 (2010)

S30 Loulergue, L. et al. Orbital and millennial-scale features of atmospheric CH_4 over the past 800,000 years. *Nature* **453,** 383-386 (2008)

Table S1 : Results from a Rampfit analysis to quantify the start, mid slope and end of Termination II increases in δD, accumulation rate (in the ice depth), $\delta^{15}N$ and δD shifted by Δdepth, atmospheric CO_2 concentration and CO_2 radiative forcing (in the gas depth). All depths and the associated uncertainties are reported in meters of ice.

units: meters	depth_bot	uncertainty	depth_top	uncertainty	depth_mid	uncertainty
δD	1771.5	4.1	1712.7	3.1	1742.8	1.8
accumulation rate	1766	5.6	1714.9	5.9	1740.5	3.1
$\delta^{15}N$	1793	2.9	1749	2.1	1771	1.8
δD shifted by Δdepth	1791.4	4.4	1747.3	3	1769.4	1.9
CO_2	1796.8	2.7	1724.8	3.6	1760.8	1.8
CO_2 forcing	1801.8	3.1	1724.8	3.8	1763.3	1.9

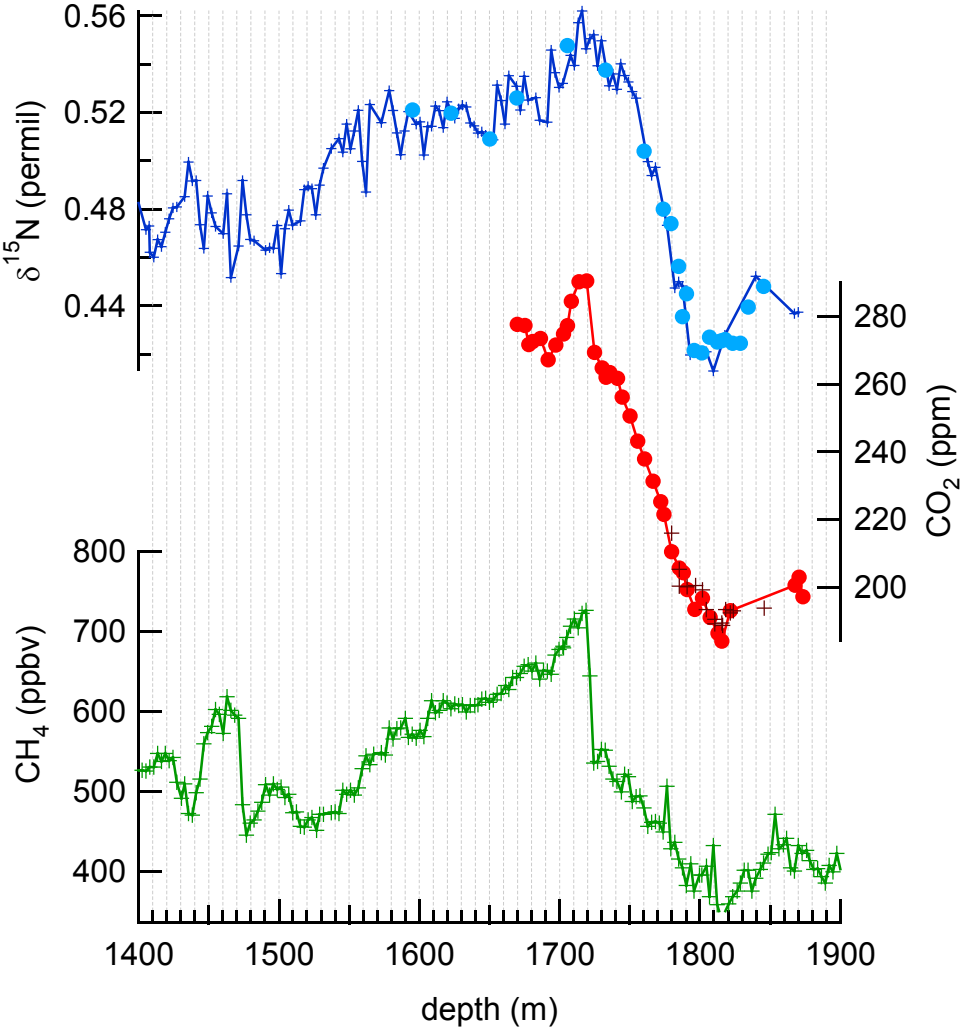

Figure S1 :

Top: new $\delta^{15}N$ data (blue crosses) and previously published $\delta^{15}N$ data (blue circles[S7]) from the EDC ice core. The analytical accuracy of replicate measurements is 6 per meg.

Middle: new CO_2 data (brown crosses) and previously published CO_2 data (red circles[S9]) from the EDC ice core.

Bottom: Atmospheric CH_4 concentrations (ppbv) from EDC[S30]

.

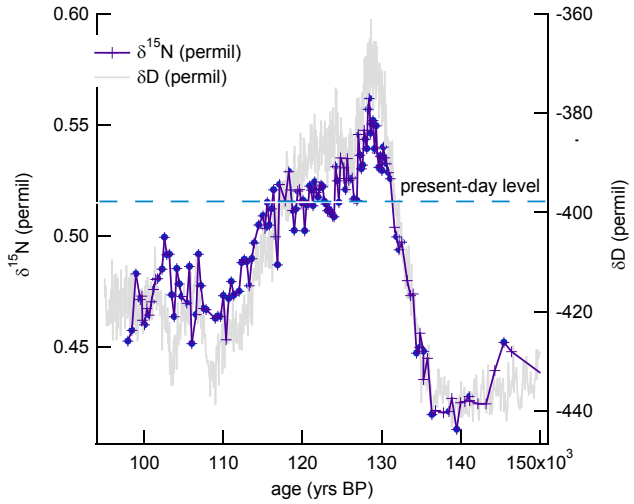

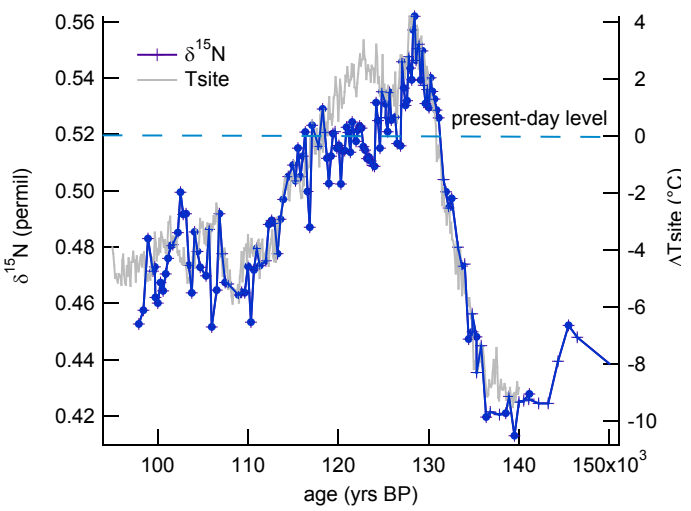

Figure S2a (left):

Comparison of $\delta^{15}N$ and δD records on the EDC3 gas and ice timescales respectively. The vertical scales have been adjusted around the present-day levels of $\delta^{15}N$ and δD.

Figure S2b (right):

Comparison of the $\delta^{15}N$ and T_{site} records on the EDC3 timescale. The vertical scales have been adjusted around the present-day levels of $\delta^{15}N$ and T_{site}.

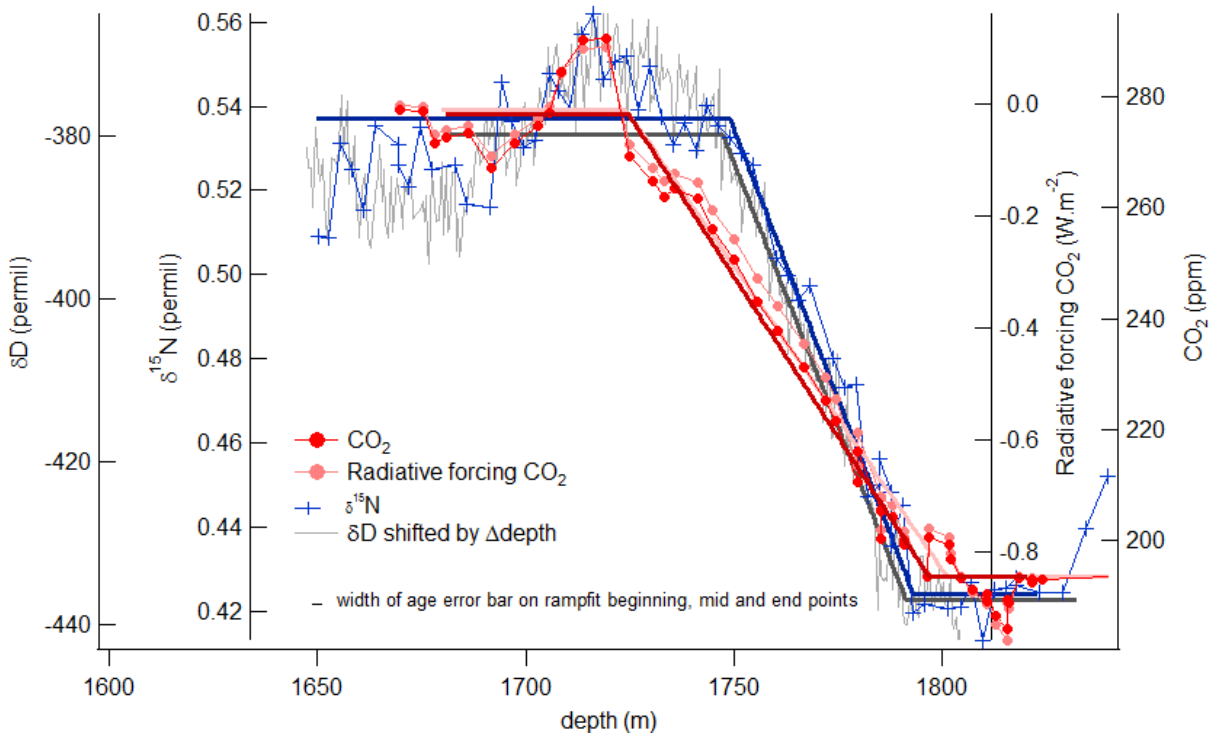

Figure S3:

Evolutions of $\delta^{15}N$ (blue), CO_2 (red), radiative forcing of CO_2 (pink) and δD shifted by Δdepth (grey) following the approach by Parrenin et al.[S4] over Termination 2. Linear segments obtained using the Rampfit software[S18] are represented as solid lines of the same color of each record.

Note that the ramp is not modified when removing the CO_2 inflexion point at 1741.3 m depth.

The radiative forcing of CO_2 is calculated following Equation (1)

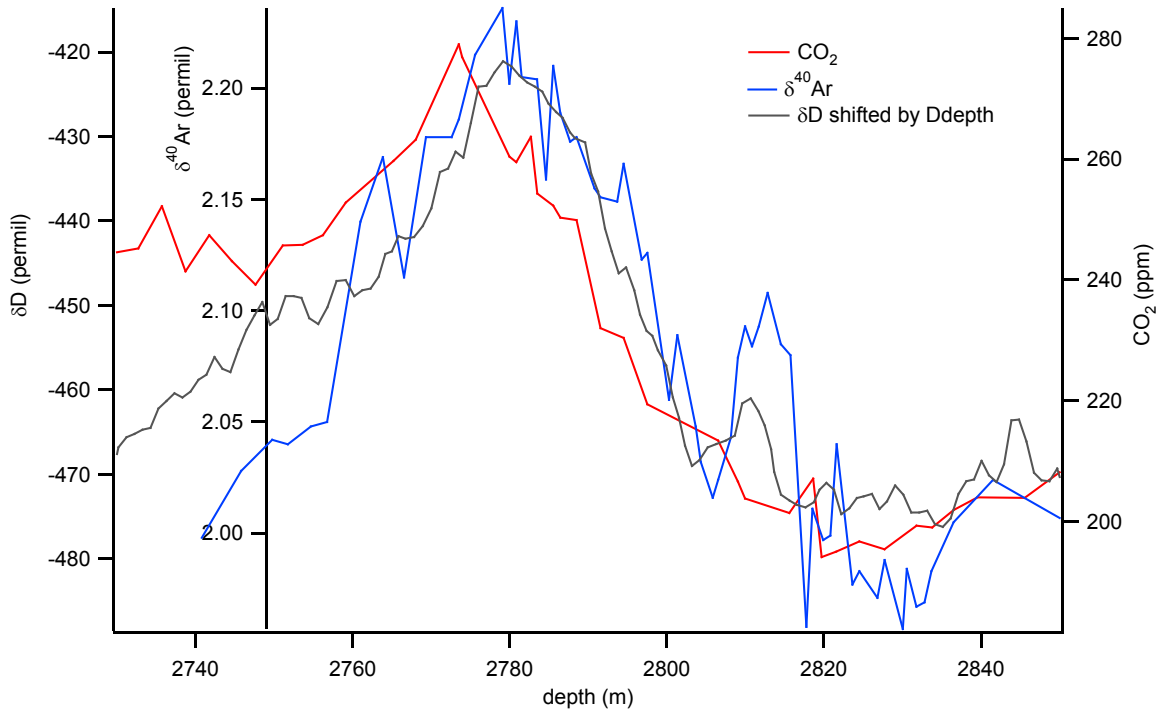

Figure S4:

Evolutions of $\delta^{40}Ar$ (blue), CO_2 (red) and δD shifted by Δdepth (grey) following the approach by Parrenin et al.[S4] over Termination II.

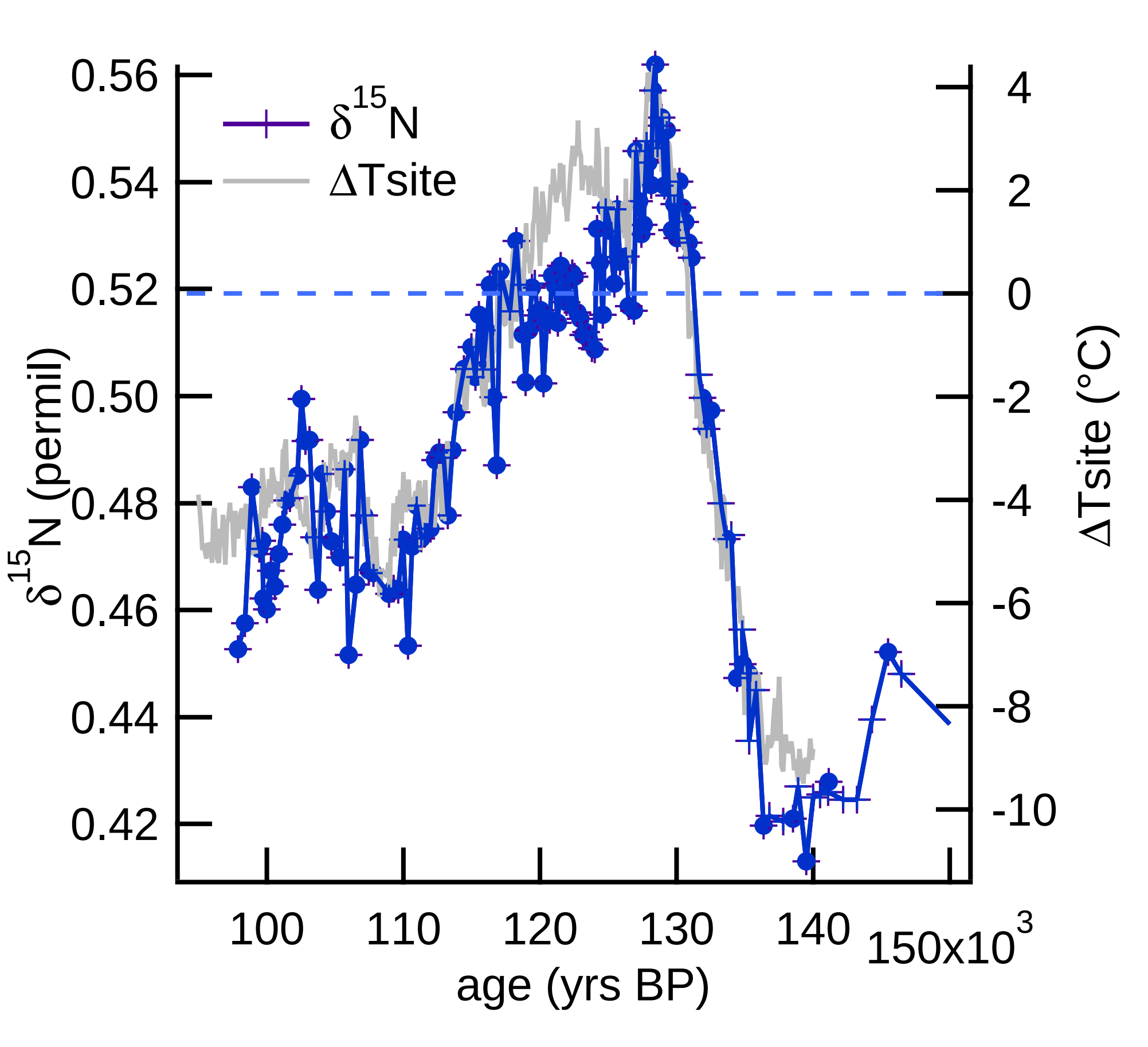
δ15N
ΔTsite
0.56
0.54
0.52
0.50
0.48
0.46
0.44
0.42
δ15N (permil)
4
2
0
-2
-4
-6
-8
-10
ΔTsite (°C)
100
110
120
130
140
150x10^3
age (yrs BP)

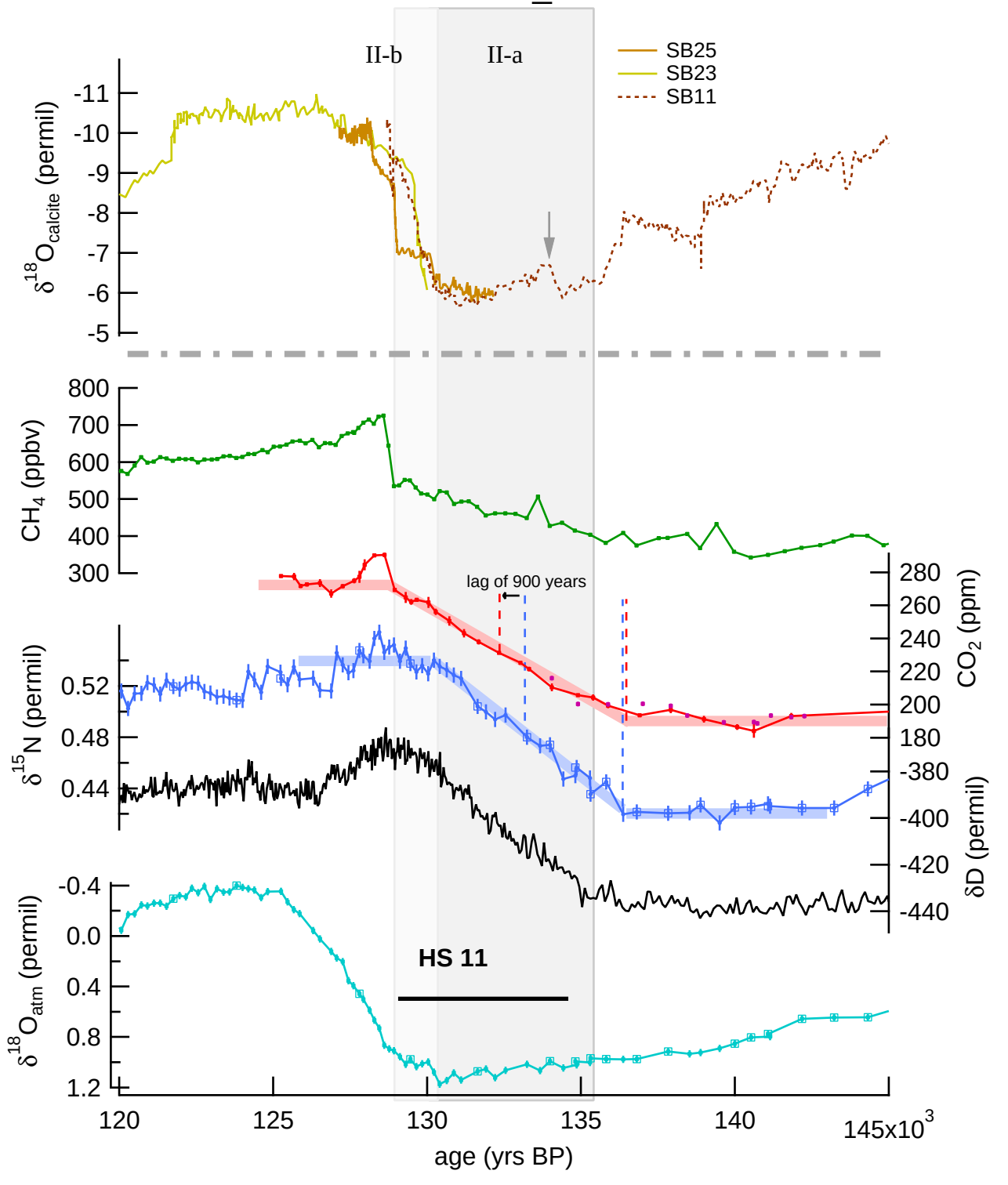
II-b
II-a
SB25
SB23
SB11
δ18Ocalcite (permil)
-11
-10
-9
-8
-7
-6
-5
CH4 (ppbv)
800
700
600
500
400
300
lag of 900 years
δ15N (permil)
0.52
0.48
0.44
CO2 (ppm)
280
260
240
220
200
180
δD (permil)
-380
-400
-420
-440
δ18Oatm (permil)
-0.4
0.0
0.4
0.8
1.2
HS 11
120
125
130
135
140
145x10^3
age (yrs BP)

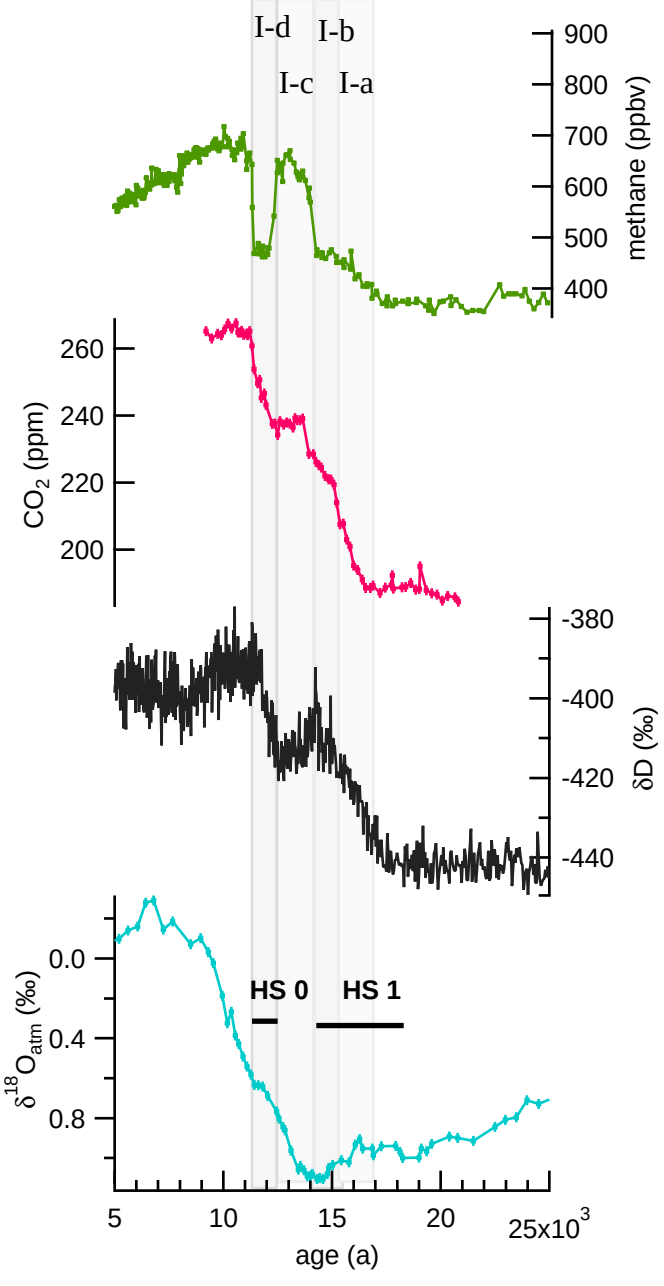
I-d
I-c
I-b
I-a
900
800
700
600
500
400
methane (ppbv)
260
240
220
200
CO2 (ppm)
-380
-400
-420
-440
δD (‰)
0.0
0.4
0.8
δ18Oatm (‰)
HS 0
HS 1
5
10
15
20
25x10^3
age (a)